Computational Visual Media
DOI 10.1007/s41095-xxx-xxxx-x Vol. x, No. x, mouth year, xx–xx

Article Type (Research/Review)

# Analyzing surface sampling patterns using the localized pair correlation function

**Weize Quan[1], Jianwei Guo[1], Dong-Ming Yan[1](✉), and Xiaopeng Zhang[1]**



**Abstract** Point distributions with different characteristics have a crucial influence on graphic applications. Various analysis tools mainly for blue noise sampling in Euclidean domains have been developed in recent years. In this paper, we present a new method to analyze the properties of general sampling patterns that are distributed on mesh surfaces. The core idea is to generalize the pair correlation function (PCF) to surfaces because the PCF has been successfully employed in sampling pattern analysis and syntheses in 2D and 3D. Experimental results demonstrate that the proposed approach can reveal the correlations of point sets generated by a wide range of sampling algorithms. An acceleration technique is also suggested to improve the performance of the PCF.

**Keywords** Point distribution, Spectral analysis, Pair correlation function, Mesh surface.

## 1 Introduction

Sampling is a fundamental research topic in computer graphics, and it has a variety of applications. Sampled point sets with specific properties are often suitable for specific applications. For example, the well-known blue noise sampling is usually used in non-photorealistic rendering [16], stippling [9], and object distribution [7]; while white noise sampling is preferred in random number generators [23]; and pink noise is used for physical simulation and biological distributions [17].

1 NLPR-LIAMA, Institute of Automation, Chinese Academy of Sciences, Beijing 100190, China. E-mail: qweizework@gmail.com, jianwei.guo@nlpr.ia.ac.cn, yandongming@gmail.com, xiaopeng.zhang@ia.ac.cn.

Several analysis tools have been proposed to evaluate the sampling properties. Some tools are performed in the spatial domain; an example is the relative radius [12], which is the normalized minimum spacing between pairs of samples. Another important tool is spectral evaluation either via the power spectrum analysis determined by Fourier transform [12, 19, 24] or via the differential domain analysis (DDA) [25]. As these tools are limited to blue noise sampling, they cannot characterize the distributions with complex sample patterns, including those that exist in many nature phenomena. Recently, Öztireli and Gross [18] proposed the use of the pair correlation function (PCF) to achieve a general analysis in 2D or 3D Euclidean spaces. However, the application of this approach in surface sampling remains unclear.

In this paper, we present a new method for analyzing surface sampling patterns using the PCF. The proposed approach is an extension of the original approach presented in [18]. The main contributions of this work include the following:

- A new approach is proposed to measure sampling properties on surfaces.
- Instead of utiziling the global PCF, the PCF method [18] is accelerated by using a localized version based on the smoothness of the Gaussian function.
- A complete comparison of recent (blue noise) sampling techniques on surfaces is performed.

## 2 Related work

This work is mostly related to surface sampling and pattern analysis. This section briefly reviews recent approaches in these two aspects.

### 2.1 Sampling

In probabilistic theory, point processes are well-studied objects, and they are powerful modeling and analysis tools for spatial data. Point processes have

been extensively researched in many disciplines, such as astronomy, chemistry, geography, and physics. A point process is a type of random process, and a particular sampling set can be regarded as a realization of such process, e.g., Poisson sampling as the realization of the Poisson process. The PCF or radial distribution function, which is a measure of the probability of finding a point at a specific distance away from a given reference point, is sufficient to describe the diverse properties of point distribution from the statistical perspective, and this measure can be used to define new analysis tools of general sampling in computer graphics [18].

Although sampling has been extensively studied in computer graphics [6, 14–16], focus is generally directed toward blue noise sampling; blue noise is a type of noise with minimal low frequency components and no concentrated spikes in energy. Blue noise sampling tends to generate sample patterns in which the points are randomly distributed at a minimum distance from one another. In this section, we only discuss a number of surface sampling algorithms. An extensive survey of blue noise sampling techniques was presented by Lagae and Dutré [12], and Yan et al. [29]. The classic dart-throwing algorithm was first generalized to mesh surfaces by Cline et al. [5]. Yan and Wonka [31] recently presented maximal Poisson-disk sampling (MPS) on surfaces based on the empty region analysis. Guo et al. [10] then improved the sampling quality and efficiency of MPS by using a hierarchical subdivision based approach. Iterative relaxation is another important technique for generating high-quality point distributions. Xu et al. [27] generalized the CCVT [2] to surfaces with potential regularity artifacts. Chen et al. [4] combined the centroidal Voronoi tessellation (CVT) [30] and CCVT for surface blue noise sampling; such combination can significantly reduce regularity artifacts by introducing the CapCVT energy. Farthest point sampling based on geodesic distance was demonstrated in [13]. In [28], the quality of blue noise sampling was further improved by extending farthest point optimization (FPO) [14, 20] to surfaces.

## 2.2 Sampling Pattern Analysis

Spatial statistics is a valid measure to analyze the spatial distribution properties of samples. Shirley [21] introduced a discrepancy to measure the quality of samples, with a small discrepancy value introduced for very equidistributed sample sets and a large discrepancy value introduced for poorly distributed sets. Liu *et al.* [13] defined a measure related to the coefficient of variation. This measure can stably analyze different point patterns on triangulated two-manifold meshes on the basis of the Voronoi diagram computed using geodesic distance. Another prevalent statistics is the relative radius, that is, the normalized minimum spacing between pairs of samples [12], which is used to analyze the spatial uniformity of Poisson disk distributions. However, this measure is only applicable in a uniform Euclidean domain. Thus, Wei and Wang [25] further extended this measure to non-uniform domains. From the perspective of point processes, Öztireli and Gross [18] defined a new analysis tool based on the PCF which measures the probability of finding a point at a specific distance away from a given point. They demonstrated that the PCF can be employed to analyze and synthesize general point distributions. However, this approach is applicable only in Euclidean domain sampling. In the present work, we generalize this approach to uniform and adaptive surface sampling. Other spatial measures are often used in recent meshing/re-meshing studies; these measures include the triangle qualities, the minimum and histogram of triangle angles, and so on [31].

Spectral analysis is another standard evaluation method that is effective in detecting sampling artifacts. Power spectrum was introduced by Ulichney [24] to study dither patterns and then used by Lagae *et al.* [12] to compare different Poisson-disk sampling methods. The power spectrum, radially averaged power spectrum, and anisotropy help to reveal point-to-point correlations. Schlömer *et al.* [19] investigated accuracy issues by computing Fourier transform analytically. Heck *et al.* [11] emphasized the shape of the power spectrum and synthesized two new types of blue noise patterns. Subr *et al.* [22] proposed to analyze the quality of samples in image synthesis by utilizing the amplitude and variance of the sampling spectrum. However, these approaches can handle only Euclidean domain sampling. Bowers *et al.* [3] was the first to propose a method for analyzing the spectral quality of surface samples, but this method can only be used for uniform sampling and analysis of a few hundred samples because of the limit of numerical computation. Recently, Wei and Wang [25] introduced the DDA to extend the standard Fourier analysis to non-uniform samples on surfaces. They replaced the cosine kernel in the definition of the Fourier power spectrum with a Gaussian kernel with the aid of the so-called pairwise sample location differentials.

## 3 Pair Correlation Function

This section briefly reviews the PCF defined in the Euclidean domain. A localized version of the PCF based on the smoothness of the Gaussian kernel is then proposed. The localized PCF is generalized to analyze adaptive samplings.

**Definition:** In contrast to that in traditional spectral analysis, the PCF is directly measured according to the spatial distance distribution of points. Specifically, it describes the joint probability of points existing at specific locations and can thus reflect the uniformity and irregularity (or randomness) of a point distribution. This measure can be used in arbitrary dimensional Euclidean space. Without loss of generality, we give its definition in a 2D case. Given a sampling point set $\mathbf{X} = \{\mathbf{x}_i\}^n$ and a sampling domain $V$, we denote $d(\mathbf{x}_i, \mathbf{x}_j)$ as the Euclidean distance between points $\mathbf{x}_i$ and $\mathbf{x}_j$, and $|V|$ as the volume of the sampling domain. The estimator of the PCF is then defined as:

$$\begin{aligned} \hat{G}_i(r) &= \frac{|V|}{2\pi r n} \sum_{j \neq i} k_\sigma(r - d(\mathbf{x}_i, \mathbf{x}_j)), \\ \hat{G}(r) &= \frac{1}{n} \sum_i \hat{G}_i(r), \end{aligned} \tag{1}$$

where $k_\sigma(x) = \frac{1}{\sqrt{\pi}\sigma} e^{-x^2/\sigma^2}$ is the Gaussian kernel. For Poisson sampling, each point is stochastically independent of all other points; hence, $\hat{G}(r) = 1$. The space where the discretization of $\hat{G}_i(r)$ (e.g., Eq. (4)) lives is called the pair correlation space (PCS). The PCS is a rigid motion invariant because it only relies on the spatial distance distribution of points. Different point sets can be mapped into the same space with the same discretization for $r$, and the properties of the point sets can be examined by analyzing the distribution of these discrete vectors (i.e., the discretization of $\hat{G}_i(r)$ with respect to $r$). For a given radius $r = r_k$, the estimator of $\hat{G}(r_k)$ can be obtained by calculating the mean of $\hat{G}_i(r_k)(i = 1, \ldots, n)$. In accordance with the observation that considerable regularity in point distributions leads to little variance in the PCS, the irregularity of point distribution can be measured by the variance of $\hat{G}_i(r_k)$ for a given radius $r = r_k$. Irregularity describes the irregularity degree of distance distribution of point sets. If points have almost the same neighbor point distribution, e.g., the point set of a regular grid, then the irregularity is small. By contrast, a random point set where each point has a different neighbor point distribution leads to large irregularity.

### 3.1 Localized PCF

The original approach [18] estimates the PCF using all pairwise distances of a point set; thus, the time complexity is $O(N^2)$, where $N$ is the number of sampling points. The time cost increases dramatically when the number of samples increases. This section proposes a localized version of the PCF to improve its performance. The localized version is $\hat{G}_i(r) = \frac{|V|}{2\pi r M} \sum_{j=1}^{M} k_\sigma(r - d(\mathbf{x}_i, \mathbf{x}_j))$. This extension is reasonable because of the smoothness of the Gauissan kernel. Intuitively, the Gaussian function introduces the weight properties into the PCF analysis. The distance $d(\mathbf{x}_i, \mathbf{x}_j)$ carries a large weight if it is close to $r$; otherwise, it carries a relatively low weight. Hence, a specific range of pairwise distances is used, i.e., the weight of $d(\mathbf{x}_i, \mathbf{x}_j)$, which is far from $r$, is set as zero. In practice, the $k$-ring neighborhood is employed to replace all pairwise distances. The time complexity of this improved version is $O(MN)$, where $M$ is the average number of points within the $k$-ring neighborhood of each sample point. In general, $M$ is much smaller than $N$ ($N \gg M$). In the most recent sampling approaches, point pairs over long distances tend to be uncorrelated; hence, the localized PCF can sufficiently capture the characteristics of these sampling patterns. To verify the validity of our new method, we compare the global PCF with our localized version and present the result in Fig. 1. We generate a set of 3,000 uniformly sampled points with the FPO method [20] as an example. When $k$ is small, the statistical pairwise distance information of one point is limited. Then, we can obtain the result of $r$ with a limited range. Interestingly, we can also capture the main peak of the PCF when $k = 1$. Along with the increase in $k$, the range of $r$ widens. We numerically calculate the difference between the localized PCF and the global one in terms of the square deviation. The results are 1.7680, 0.1288, 0.0355, 0.030, and 0.015. When $k \geq 6$, the results are almost same in both visual and numerical terms.

### 3.2 Adaptive Sampling

If an importance function $f(\mathbf{p})$ is defined in an $n$-dimensional sample domain, then the sampling becomes adaptive. The difference between uniform and adaptive sampling is that adaptive sampling introduces a weight for each point, i.e., each sample point is equipped with a weight $\mathbf{S} = \{\mathbf{p}_i, w_i\}_{i=1}^N$. The weight $w(\mathbf{p})$ of each point can be derived from the importance function $f(\mathbf{p})$ with $w(\mathbf{p}) \propto f(\mathbf{p})^{-\frac{1}{n}}$. In adaptive sampling analysis, defining a valid distance

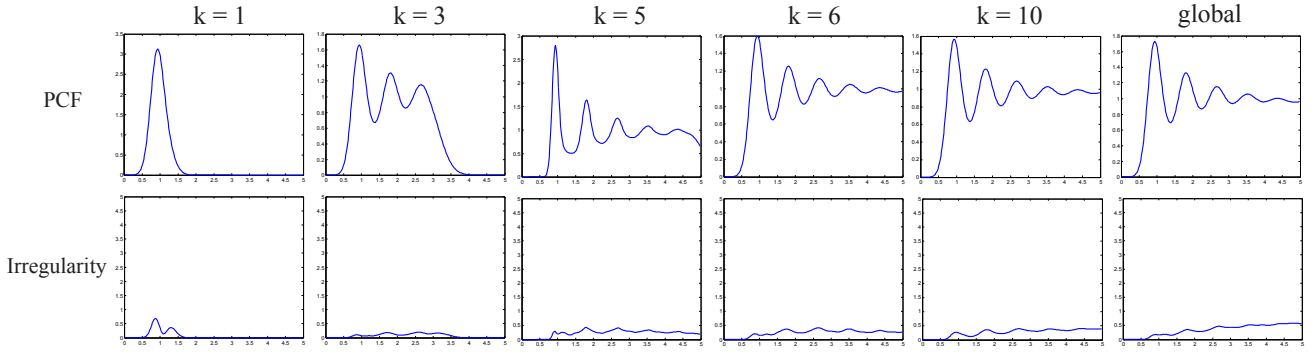


**Fig. 1** Analysis of PCF with different local neighborhood sizes. From left to right: $k = 1, 3, 5, 6, 10$, global. We use the uniform FPO method [20]. The number of samples is 3,000. $\sigma = 0.25$.

measure is an important issue. To generalize the PCF analysis method to adaptive sampling, the warp method introduced in [25] is utilized in mapping the non-uniform domain to a uniform one. The sampling points carry a large weight at flat regions in the domain and a low weight at highly-curved regions. The transformation function given in Eq.(2) is employed to approximate the uniform distance between two samples.

$$d_{ij} = \frac{2 * E(w)}{w_i + w_j} \|\mathbf{p}_i - \mathbf{p}_j\|, \tag{2}$$

where $w_i$ and $w_j$ are the weight of points $\mathbf{p}_i$ and $\mathbf{p}_j$, respectively. $E(w)$ is the mean weight of all points. Furthermore, $E(w)$ scales the pairwise distance but does not affect the shape of the PCF and Irregularity. Fig. 2 shows an example of an analysis of 2D sampling patterns using the proposed approach. As shown in the figure, the uniform and adaptive cases share the same consistent appearance in terms of the PCF and irregularity except the case of a small $\sigma$. The PCF is the probability density function of pairwise distances using kernel density estimation. Scale factor $\sigma$ decides the local estimation neighborhood size and thus plays an important role in this estimator. However, this hyper-parameter is difficult to estimate and is usually obtained through some experiments. In Fig. 2, we compare the effects of different $\sigma$ on the results. Small or large $\sigma$ values lead to inaccurate estimation. Specifically, a large $\sigma$ indicates a Poisson sampling pattern, i.e., the PCF is flat and equal to 1.

## 4 PCF on Surfaces

In this section, we propose a new approach for analyzing sampling patterns on surfaces on the basis of the localized PCF. The inputs are a two-manifold domain $\Omega$ (represented by a triangular mesh) and the corresponding sampled point sets $\mathbf{S} = \{\mathbf{p}_i\}_{i=1}^N$. The PCF on surface can be defined as:

$$g(r) = \frac{|V|}{4\pi r^2 MN} \sum_{i=1}^{N} \sum_{j=1}^{M} k_\sigma(r - d_{ij}), \tag{3}$$

where $M$ is the local neighborhood size (i.e., the number of points within the $k$-ring neighborhood of one sample point), $|V|$ is the superficial area of the model, and $d_{ij}$ is the distance between points $\mathbf{p}_i$ and $\mathbf{p}_j$. Note that the concept of the PCF could be generalised to arbitrary manifolds with a metric. However, we will focus only on the surface in this paper.

The most intuitive choice of distance metric on surfaces is geodesic distance. However, the computation of geodesic distance is still time consuming even with hardware acceleration. In many applications in which the number of sampling points increases relative to the surface curvature, the Euclidean metric becomes a suitable approximation of the geodesic distance [8] in a local neighborhood. This approximation is validated in Sec. 5 by comparing the analysis quality of using both metrics. Hence, we adopt Euclidean distance in our approach, i.e., $d_{ij} = \|\mathbf{p}_i - \mathbf{p}_j\|$ in uniform sampling. To make $g(r)$ independent of the point number $N$, we further normalize $d_{ij}$ by $d_{max}$, which indicates the theoretically largest minimum distance between any two sample points. Here, $d_{max} = 2\sqrt{\frac{A}{2\sqrt{3}N}}$, and $A$ is the area of surface [32].

The PCF essentially analyzes the distance distribution of sampling points with the kernel density estimation method. In the statistical community, data distribution can be effectively characterized by the average and variance of the data. Therefore, we can reasonably regard the PCF as the average of the

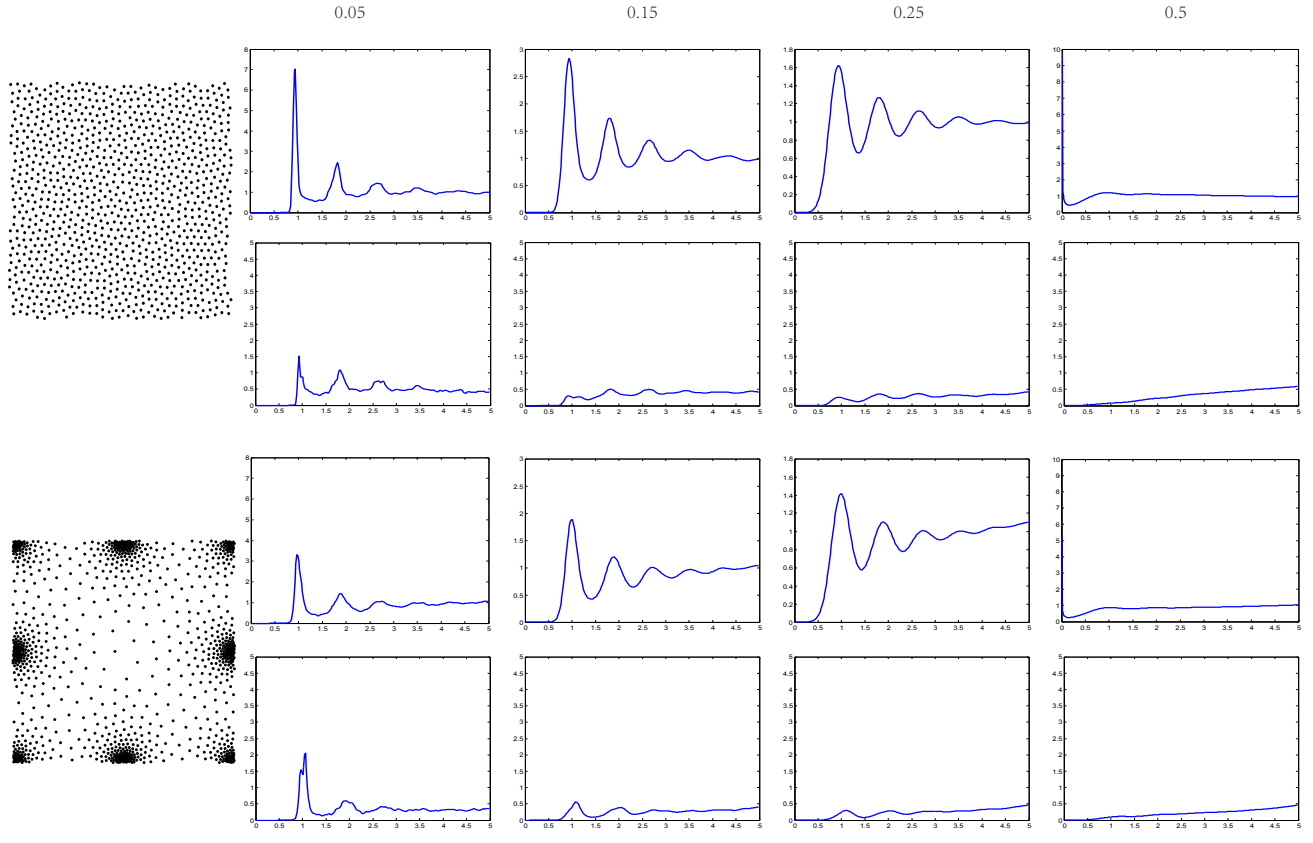


**Fig. 2** Analysis of the 2D uniform (top) and adaptive sampling (bottom). The sampling points are generated using the FPO method [20] shown in first column. The number of samples is 1,024, and the neighborhood size is $k = 10$. We set $\sigma = 0.05, 0.15, 0.25, 0.5$ from left to right.

distance distribution, i.e.,

$$g(r) = \frac{1}{N}\sum_{i=1}^{N} g_i(r), \tag{4}$$

where $g_i(r) = \frac{|V|}{4\pi r^2 M}\sum_{j=1}^{M} k_\sigma(r - d_{ij})$. In practice, the discrete PCF is used by discretizing $r$, i.e., $\mathbf{r} = (r_1, r_2, \cdots, r_k)^T$. Therefore, $g(r)$ and $g_i(r)$ can be discretized as follows:

$$\begin{aligned} \Phi &= (g(r_1), g(r_2), \cdots, g(r_k))^T; \\ \Phi_i &= (g_i(r_1), g_i(r_2), \cdots, g_i(r_k))^T, \end{aligned} \tag{5}$$

In addition, irregularity can be captured by the variance of the distance distribution for each sampling point. The irregularity measure can be defined as:

$$V_{r_k} = \frac{1}{N}\sum_{i=1}^{N}(\Phi_{ik} - \Phi_k)^2. \tag{6}$$

For normalization, this measure is divided by the irregularity of white noise samplings.

For a given 3D mesh and its corresponding sample points, we first triangulate the point set using the restricted Delaunay triangulation [30] to compute the local distance for each point using the breadth first search. For each $r_k$, $\Phi_{ik}$ is computed for each point. Then, the corresponding $\Phi_k$ and $V_{r_k}$ is calculated. The core steps of computing PCF and Irregularity are shown in Algorithm 1. Consequently, the adaptive PCF and Irregularity on the surface can be easily obtained by replacing $\|\mathbf{p}_i - \mathbf{p}_j\|$ with $\frac{2*E(w)}{w_i+w_j}\|\mathbf{p}_i - \mathbf{p}_j\|$ when computing $\Phi_{ik}$ in Alg. 1.

**Algorithm 1** Computing PCF and Irregularity

**Input:** 3D mesh, Sampling set **S**.
**Output:** PCF and Irregularity of **S**.
**Initialize:** PCF and Irregularity of **S**
**for all** $r_k \in \mathbf{r}$ **do**
  **for all** $\mathbf{p}_i \in \mathbf{S}$ **do**
    compute $\Phi_{ik}$
  **end for**
  compute $\Phi_k$ and $V_{r_k}$
**end for**

## 5 Experimental Results

We present our experimental results on different sampling patterns to verify the validity of the proposed

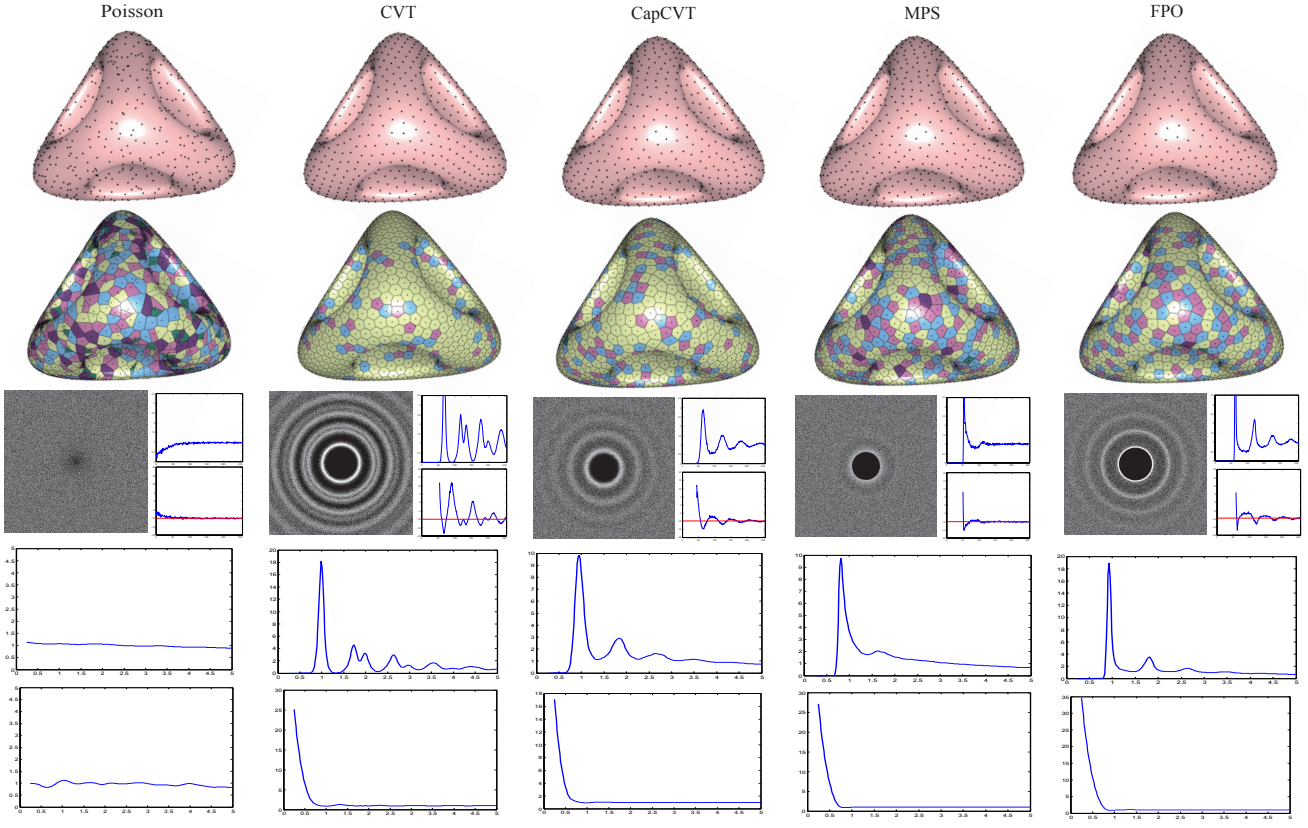


**Fig. 3** Analysis of different point distributions on a uniform domain. From top to bottom: surface sampling results; Voronoi cells (each cell is color-coded by its valence: light yellow is valence 6, pink is valence 5, and blue is valence 7; dark pink is valence larger than 7, and dark green is valence smaller than 5); DDA analysis [25], including the power spectrum, radial mean, and anisotropy; our PCF results; and our irregularity measures. We set $\sigma = 0.05, k = 7$.

method. All the results shown in this work are obtained with a PC equipped with 2.83 GHz Q9550 Quad CPU, 4 GB memory, and 64-bit Windows 7 operating system.

**Parameters:** The most important parameter is the neighborhood size $M$ of each point, which directly affects the speed and quality of our algorithm. Neighborhood size is related to the number of sampling points. In our tests, we adapt $k$ to match the neighborhood size. When the number of samples is large, we increase $k$ accordingly to collect adequate neighborhood information. Furthermore, a large $M$ does not change the shape of the PCF but affects the Irregularity. In our experiments, we find that $k \in [5, 15]$ is generally effective. We set $k = 7$ for our results unless explicitly specified. Given the range $[r_1, r_2]$ of r values and $\sigma$ value, the maximum neighborhood size in terms of pairwise distance is $D = d_{max}(r_2 + \mu\sigma)$, where $\mu$ is the cutoff factor of the Gaussian function. Using this formulation, we can estimate a good $k$ and qualify the reasonableness of a given $k$ as well.

Another important parameter is the standard deviation $\sigma$ of the Gaussian kernel, which affects the smoothness of the result. In the uniform surface sampling, we find $\sigma \in [0.04, 0.08]$ to be effective, and we set $\sigma = 0.05$. In the adaptive surface sampling, we find $\sigma \in [0.06, 0.12]$ to be effective, and we set $\sigma = 0.08$. The range of $\mathbf{r}$ should capture adequate information on the point distribution. In our tests, $\mathbf{r} \in [0.25, 5]$, and the stride of 0.02 can obtain the tradeoff between smoothness and efficiency.

**Performance:** As shown in Fig. 4, we compare the running time of the original PCF and our localized version. We use the increasing number of points and test the running time separately. The sampling points of varying amounts are obtained with the CCVT method [2], and the number of points in each site is 1,024. The speed of the localized PCF is significantly faster than that of the global PCF. Specifically, the running time of the global PCF is quadratic with respect to the number of sampling points, whereas that of the localized PCF is almost linear.

**Sampling analysis:** We apply our approach to

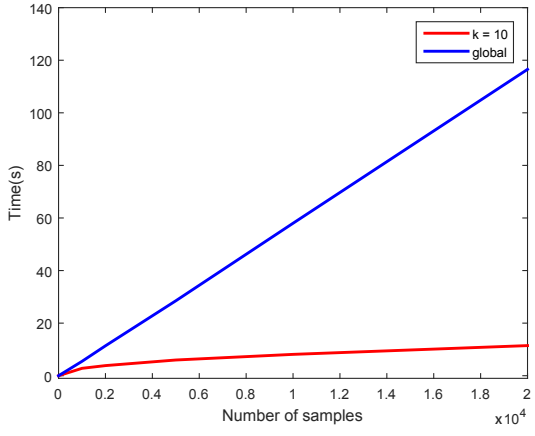


**Fig. 4** Comparison of running time of our local distance measure and the original one [18]. Time is the square root of the true time for clarity. The blue curve corresponds to the original global method, whereas the red curve is our localized method. We use the CCVT method [2] to generate samplings. The number of points in each site is 1,024. We set $\sigma = 0.25$ in this example.

analyze several sampling algorithms on surfaces, including CVT [30], CapCVT [4], MPS [10, 31], and FPO [28]. Poisson sampling is used for ground truth, where $g(r) = 1$. We use two new measures in our analysis, i.e., $P_{peak}$ and $I_{valley}$, which are obtained from our PCF and irregularity analysis. The value of $P_{peak}$ indicates the specific distance at which most points are distributed with respect to their neighborhood points. In other words, most points have a similar distribution in this specific distance. Thus, the irregularity is relatively small. Hence, $P_{peak}$ and $I_{valley}$ are almost the same. We also observe that $P_{peak}$ is essentially equivalent to the average relative radius $\rho$ defined in [12]; however, this measure cannot be obtained from DDA directly. For example, $P_{peak}$ of FPO is close to 0.93, and $P_{peak}$ of MPS is approximately 0.81; these values agree well with the reported values in [20]. Furthermore, these two measures are independent of the number of samples and the area of the sampling domain because we normalize the distance measure by $d_{max}$. Thus our approach has strong generalization ability. The results are shown in Fig. 3, and the values of these measures are shown in Tab. 1.

For adaptive sampling (non-uniform density sampling), we transform the adaptive domain to a uniform case using the weight information defined in each point and directly apply the uniform analysis tools. To ensure the validity of the transformation function of Eq.(2), we apply our algorithm to the adaptive version of four sampling algorithms on surfaces(Fig. 5). Poisson sampling is employed for ground truth as well. The results are almost the same as the uniform results shown in Fig. 3.

**Tab. 1** Statistics of PCF and irregularity. $|\mathbf{S}|$ is the number of sampled points. $P_{peak}$ is the abscissa of the main peak of PCF. $I_{valley}$ is the abscissa of the valley of irregularity. The abscissa value of 2 denotes true distance $2d_{max}$ because of the normalization of distance.

| Model | Method | $\|\mathbf{S}\|$ | $P_{peak}$ | $I_{valley}$ |
|---|---|---|---|---|
| Eight | CVT | 1.7K | 0.99 | 1.01 |
| | CapCVT | 1.7K | 0.95 | 0.97 |
| | MPS | 1.7K | 0.81 | 0.79 |
| | FPO | 1.7K | 0.93 | 0.93 |
| Genus | CVT | 6.2K | 0.99 | 1.01 |
| | CapCVT | 6.2K | 0.95 | 0.97 |
| | MPS | 6.2K | 0.81 | 0.79 |
| | FPO | 6.2K | 0.93 | 0.89 |
| Kitten | CVT | 2.9K | 0.99 | 1.01 |
| | CapCVT | 2.9K | 0.95 | 0.97 |
| | MPS | 2.9K | 0.81 | 0.79 |
| | FPO | 2.9K | 0.93 | 0.89 |

To demonstrate the effectiveness of our analysis method in models with different topological structures, we persent the results of our approach applied to several models with different topological structures(Fig. 6). We obtain the sample points by MPS. The left column indicates the uniform sampling, and the right column shows the adaptive sampling. For adaptive MPS sampling, we use the local feature size (lfs) [1] as the sizing function. We can find that uniform and adaptive cases exhibit a consistent appearance, including the PCF and irregularity. Furthermore, our method can capture the blue noise property of this pattern, in which the PCF features a salient peak for each model.

**Comparison with DDA:** We also compare our method with the DDA tool [25](Fig. 3). The core principle of DDA is to use the distribution of difference vectors $\mathbf{p}_i - \mathbf{p}_j$. Our PCF is based on the probability analysis of the magnitude of difference vectors, i.e., $\|\mathbf{p}_i - \mathbf{p}_j\|$. The PCF contains the same information as the radial average of the DDA. As shown in Fig. 3, the radial mean of the DDA is consistent with our PCF. In essence, the DDA performs the kernel density estimation of $p(\mathbf{d})$ (the probability density function of $\mathbf{d}$), and $p(\mathbf{d})$ is constructed from a straightforward histogram. The PCF is $p(|\mathbf{d}|)$ using the Gaussian function. In addition, we analyze the irregularity of the point distribution instead of anisotropy because pairwise distance $|\mathbf{d}|$ has no directional information. For example, the radial mean and PCF of CapCVT

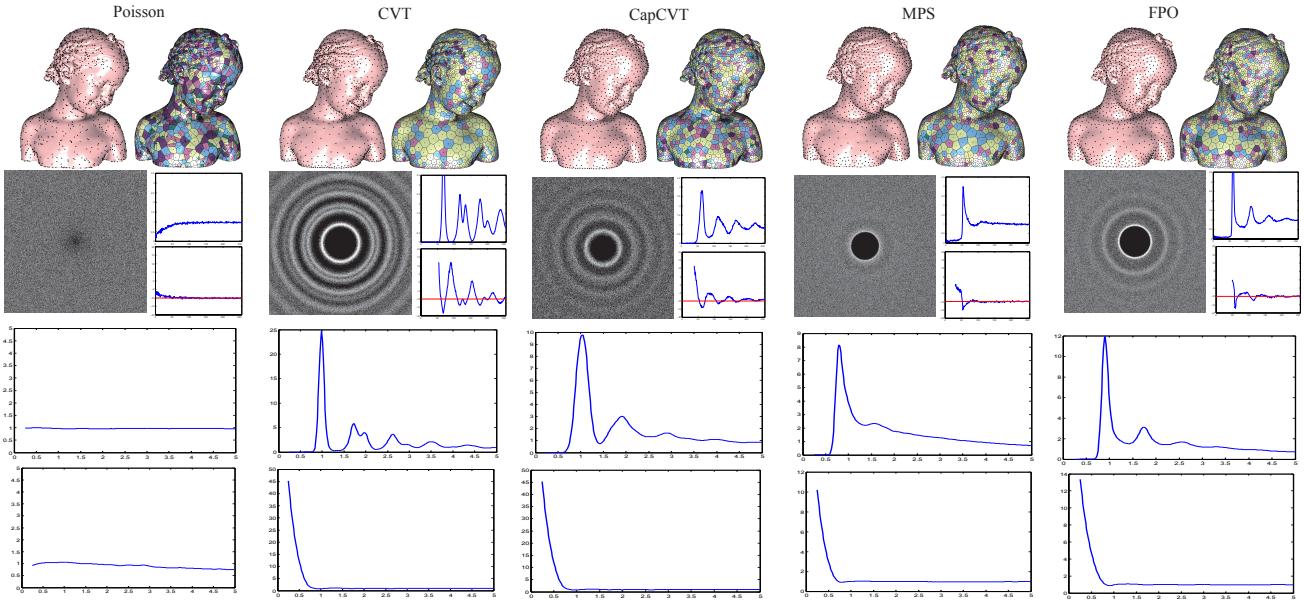


**Fig. 5** Analysis of different point distributions on the adaptive domain. We set $\sigma = 0.08, k = 7$.

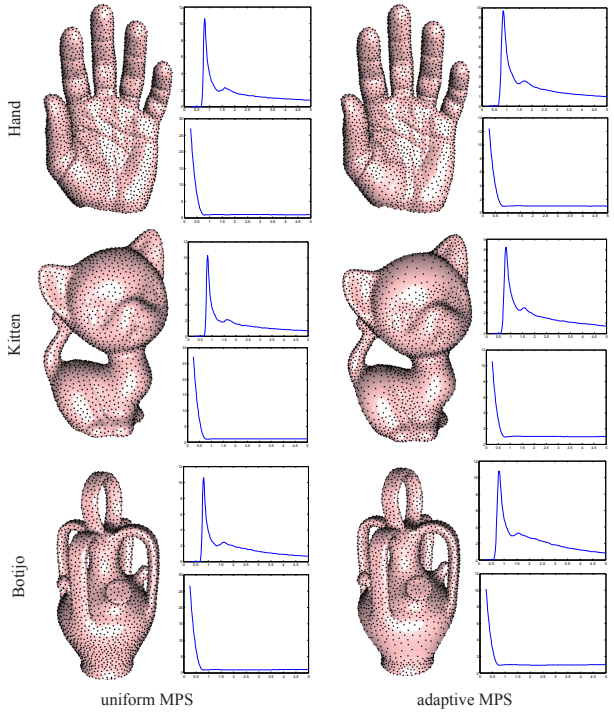


**Fig. 6** Analysis of uniform and adaptive sampling in different models. The left column is uniform sampling, whereas the right column is adaptive sampling. Each group includes surface sampling results, PCF results, and irregularity measures. The number of sampling points is approximately 3,000. We set $\sigma = 0.05$ for uniform sampling and $\sigma = 0.08$ for adaptive sampling. $k = 7$.

both exhibit visible fluctuations. In addition, the PCF can further reveal the distance characteristics because it is a statistical measure based on pairwise distances. Fig. 3 shows that the PCF of Poisson sampling is flat because of the uniformity of the distance distribution. The other four methods show apparent main peaks in the PCF. The PCF of CVT exhibits a larger fluctuation after the main peak in comparison with the other three methods. The irregularity of CVT has a low-lying area which indicates that CVT has high regularity. The irregularity of MPS is flatter than that of the other three methods; hence, MPS has good blue noise properties.

In sampling, regularity is an important criterion that inherently presents a potential risk for aliasing. Our method can analyze the regularity degree of a sampling pattern, which cannot be obtained with the DDA tool [25]. CapCVT [4] adopts parameter $\lambda$ to balance regularity and randomness. Decreasing $\lambda$ introduces regular patterns. The patterns are the same as that of CVT if $\lambda = 0$. When $\lambda$ increases, the point distribution shows irregularities, which are the core principle of CapCVT to avoid the regular patterns observed in CVT. In Fig. 7, we show our analysis results by applying our algorithm to the samples generated by CapCVT with different $\lambda$. The number of samples is $3,000$. The first column is similar to the PCF of CVT because $\lambda$ is very small, and the residual of the other three PCFs is almost same. However, the Irregularity shows more fluctuations from left to right, i.e., more randomness, which is consistent with the

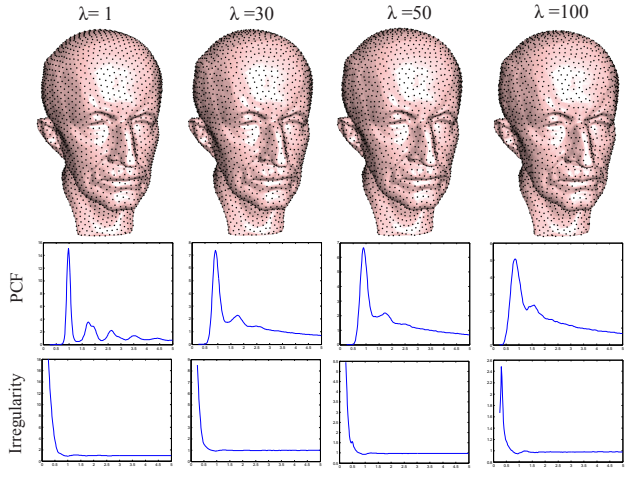


**Fig. 7** Analysis of CapCVT [4] with different $\lambda$ (from left to right, $\lambda = 1, 30, 50, 100$). From top to bottom: surface sampling results, PCF results, and irregularity measures. The number of samples is 3,000, $\sigma = 0.05$, and $k = 7$.

result of CapCVT [4].

**Euclidean vs geodesic:** To verify that the Euclidean metric is a suitable approximation for PCF analysis on surfaces, we compare the analysis results of both metrics(Fig. 8). In our experiments, we employ the fastest MMP algorithm [26] for geodesic computation. When the number of points is small, the result of using the Euclidean metric is slightly biased because the approximation error is too large. When the number of points increases, the results of the two metrics become similar. Note that the results of both metrics become smooth when the number of samples increases.

**Limitations:** Our current approach has several limitations. For example, we only focus on analyzing isotropic sampling patterns and do not address the anisotropic sampling. Another limitation is that the local neighborhood distance computation depends on the restricted Delaunay triangulation of the sampling points and may thus be problematic in regions with inadequate samples. We aim to address these issues in our future work.

## 6 Conclusions

We proposed a localized version of the PCF to accelerate the algorithm without reducing the quality of analysis. We generalized the PCF to analyze the sampling patterns on surfaces. The experimental results demonstrate that our method can determine the properties of different point distributions. In the future, we aim to develop new techniques for point sampling synthesis on surfaces. We also plan to increase the speed of our algorithm using GPU because of its local characteristics.

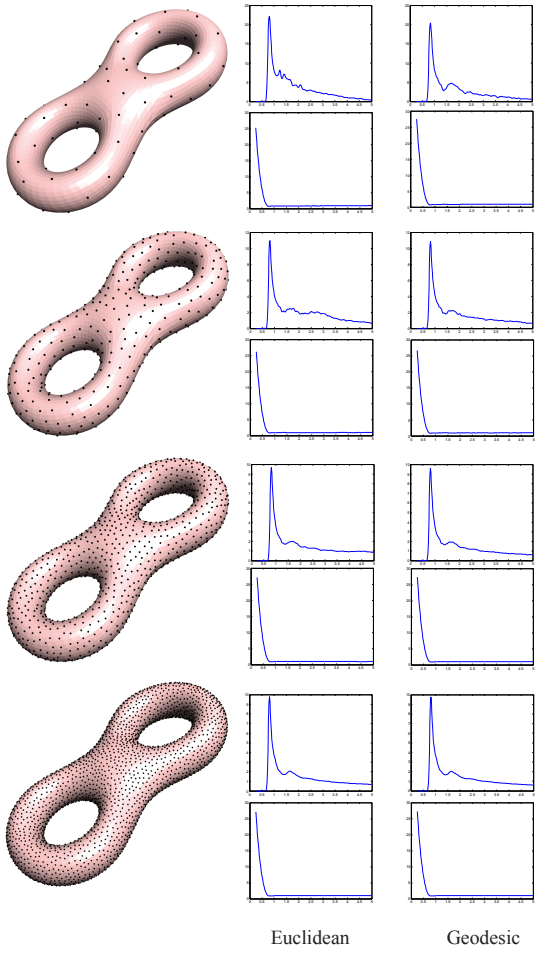


**Fig. 8** Comparison of analysis results using Euclidean and geodesic metrics. Left column: surface sampling results, middle column: results of using Euclidean metric, right column: results of geodesic metric. Each row includes our PCF results and irregularity measures. From top to bottom, the number of sampling points is 100, 500, 1,500, and 3,500, as generated by MPS [31]. We set $\sigma = 0.05, k = 7$.

## References

[1] N. Amenta, M. Bern, and M. Kamvysselis. A new Voronoi-based surface reconstruction algorithm. In *Proc. ACM SIGGRAPH*, pages 415–421, 1998.

[2] M. Balzer, T. Schlömer, and O. Deussen. Capacity-constrained point distributions: A variant of Lloyd's method. *ACM Trans. on Graphics (Proc. SIGGRAPH)*, 28(6):86:1–86:8, 2009.

[3] J. Bowers, R. Wang, L.-Y. Wei, and D. Maletz. Parallel Poisson disk sampling with spectrum analysis on surfaces. *ACM Trans. on Graphics (Proc. SIGGRAPH Asia)*, 29(6):166:1–166:10,

2010.

[4] Z. Chen, Z. Yuan, Y.-K. Choi, L. Liu, and W. Wang. Variational blue noise sampling. *IEEE Trans. on Vis. and Comp. Graphics*, 18(10):1784–1796, 2012.

[5] D. Cline, S. Jeschke, A. Razdan, K. White, and P. Wonka. Dart throwing on surfaces. *Computer Graphics Forum (Proc. EGSR)*, 28(4):1217–1226, 2009.

[6] R. L. Cook. Stochastic sampling in computer graphics. *ACM Trans. on Graphics*, 5(1):69–78, 1986.

[7] O. Deussen, P. Hanrahan, B. Lintermann, R. Mech, M. Pharr, and P. Prusinkiewicz. Realistic modeling and rendering of plant ecosystems. *Proc. ACM SIGGRAPH*, pages 275–286, 1998.

[8] Q. Du, M. D. Gunzburger, and L. Ju. Constrained centroidal Voronoi tesselations for surfaces. *SIAM J. SCI. COMPUT.*, 24(5):1488–1506, 2003.

[9] R. Fattal. Blue-noise point sampling using kernel density model. *ACM Trans. on Graphics (Proc. SIGGRAPH)*, 28(3):48:1–48:10, 2011.

[10] J. Guo, D.-M. Yan, X. Jia, and X. Zhang. Efficient maximal Poisson-disk sampling and remeshing on surfaces. *Computers & Graphics*, 46(6-8):72–79, 2015.

[11] D. Heck, T. Schlömer, and O. Deussen. Blue noise sampling with controlled aliasing. *ACM Trans. on Graphics*, 32(3):25:1–25:12, 2013.

[12] A. Lagae and P. Dutré. A comparison of methods for generating Poisson disk distributions. *Computer Graphics Forum*, 27(1):114–129, 2008.

[13] Y.-J. Liu, Z. Chen, and K. Tang. Construction of iso-contours, bisectors, and voronoi diagrams on triangulated surfaces. *Pattern Analysis and Machine Intelligence, IEEE Transactions on*, 33(8):1502–1517, 2011.

[14] S. A. Lloyd. Least squares quantization in PCM. *IEEE Transactions on Information Theory*, 28(2):129–137, 1982.

[15] M. McCool and E. Fiume. Hierarchical Poisson disk sampling distributions. In *Graphics Interface*, pages 94–105, 1992.

[16] D. P. Mitchell. Generating antialiased images at low sampling densities. In *Proc. ACM SIGGRAPH*, pages 65–72, 1987.

[17] A. Ostling, J. Harte, and J. Green. Self-similarity and clustering in the spatial distribution of species. *Science*, 290(5492):671–671, 2000.

[18] A. C. Öztireli and M. Gross. Analysis and synthesis of point distributions based on pair correlation. *ACM Trans. on Graphics (Proc. SIGGRAPH Asia)*, 31(6):170, 2012.

[19] T. Schlömer and O. Deussen. Accurate spectral analysis of two-dimensional point sets. *Journal of Graphics, GPU, and Game Tools*, 15(3):152–160, 2011.

[20] T. Schlömer, D. Heck, and O. Deussen. Farthest-point optimized point sets with maximized minimum distance. In *High Performance Graphics Proceedings*, pages 135–142, 2011.

[21] P. Shirley. Discrepancy as a quality measure for sample distributions. In *In Eurographics '91*, pages 183–194, 1991.

[22] K. Subr and J. Kautz. Fourier analysis of stochastic sampling strategies for assessing bias and variance in integration. *ACM Trans. on Graphics (Proc. SIGGRAPH)*, 32(4):905–914, 2013.

[23] S. Tzeng and L.-Y. Wei. Parallel white noise generation on a GPU via cryptographic hash. In *Proceedings of the 2008 symposium on Interactive 3D graphics and games*, pages 79–87. ACM, 2008.

[24] R. Ulichney. *Digital Halftoning*. MIT Press, 1987.

[25] L.-Y. Wei and R. Wang. Differential domain analysis for non-uniform sampling. *ACM Trans. on Graphics (Proc. SIGGRAPH)*, 30(4):50:1–50:8, 2011.

[26] C. Xu, T.-F. Wang-Yang, Y.-J. Liu, L. Liu, and Y. He. Fast wavefront propagation (fwp) for computing exact geodesic distances on meshes. *Visualization and Computer Graphics, IEEE Transactions on*, 21(7):822–834, 2015.

[27] Y. Xu, R. Hu, C. Gotsman, and L. Liu. Blue noise sampling of surfaces. *Computers & Graphics*, 36(4):232–240, 2012.

[28] D.-M. Yan, J. Guo, X. Jia, X. Zhang, and P. Wonka. Blue-noise remeshing with farthest point optimization. *Computer Graphics Forum (Proc. SGP)*, 33(5):167–176, 2014.

[29] D.-M. Yan, J. Guo, B. Wang, X. Zhang, and P. Wonka. A survey of blue-noise sampling and its applications. *Journal of Computer Science and Technology*, 30(3):439–452, 2015.

[30] D.-M. Yan, B. Lévy, Y. Liu, F. Sun, and W. Wang. Isotropic remeshing with fast and exact computation of restricted Voronoi diagram. *Computer Graphics Forum*, 28(5):1445–1454, 2009.

[31] D.-M. Yan and P. Wonka. Gap processing for adaptive maximal Poisson-disk sampling. *ACM Trans. on Graphics*, 32(5):148:1–148:15, 2013.

[32] C. Yuksel. Sample elimination for generating Poisson disk sample sets. *Computer Graphics*

*Forum (Proceedings of EUROGRAPHICS 2015)*, 37(2), 2015. to appear.